Divergent Features of the Tropopause Aerosol Layer: Effects of Monsoon Dynamics and Pollution Emissions in Asia, South America, and Africa

Dongyou Wu[1], Shirui Yan[1], Jinxia Zhang[1], Yang Chen[1], Yuxuan Xing[1], Jun Liu[1], Xin Wang[2], and Wei Pu[3]

[1]Lanzhou University
[2]Tianjin University
[3]

June 14, 2023

Abstract

The tropopause aerosol layer (TAL) represents the increase of aerosols in tropopause. It was first discovered over Asia but was found in this study to also occur over South America and Africa owing to the combined effects of monsoon dynamics and pollutant emissions. Over Asia, the TAL has the highest altitude and widest spread due to strong deep convection and the upper troposphere anticyclonic system there. TAL intensity is highest in South America due to heavy pollutant emissions. Anthropogenic pollution from India and western China produces two Asian TAL centers, whereas widespread wildfires result in single centers over South America and Africa. TAL radiative forcing induced by carbonaceous aerosols at the top of the atmosphere has warming effects over Asia (+0.21 W m-2), whereas cooling effects occur over South America (-0.47 W m-2) and Africa (-0.12 W m-2) owing to the divergent strengths of black-carbon absorption and organic-carbon scattering.

Hosted file

965045_0_art_file_11072276_rvytlm.docx available at https://authorea.com/users/628251/articles/648941-divergent-features-of-the-tropopause-aerosol-layer-effects-of-monsoon-dynamics-and-pollution-emissions-in-asia-south-america-and-africa

Divergent Features of the Tropopause Aerosol Layer: Effects of Monsoon Dynamics and Pollution Emissions in Asia, South America, and Africa

Dongyou Wu[1], Shirui Yan[1], Jinxia Zhang[1], Yang Chen[1], Yuxuan Xing[1], Jun Liu[1], Xin Wang[1, 2] and Wei Pu[1*]

[1] Key Laboratory for Semi-Arid Climate Change of the Ministry of Education, College of Atmospheric Sciences, Lanzhou University, Lanzhou 730000, China

[2] School of Earth System Science, Tianjin University, Tianjin 300072, China

Corresponding author: Wei Pu (puwei@lzu.edu.cn)

Key Points:

- TALs occur not only over Asia, but also over South America and Africa owing to the combined effects of monsoon dynamics and pollutant emissions.
- Strong monsoon dynamics cause the highest altitude and widest coverage of the TAL over Asia.
- TAL CAs from anthropogenic emissions cause warming effects over Asia and natural emissions cause cooling effects over South America and Africa.

Abstract

The tropopause aerosol layer (TAL) represents the increase of aerosols in tropopause. It was first discovered over Asia but was found in this study to also occur over South America and Africa owing to the combined effects of monsoon dynamics and pollutant emissions. Over Asia, the TAL has the highest altitude and widest spread due to strong deep convection and the upper troposphere anticyclonic system there. TAL intensity is highest in South America due to heavy pollutant emissions. Anthropogenic pollution from India and western China produces two Asian TAL centers, whereas widespread wildfires result in single centers over South America and Africa. TAL radiative forcing induced by carbonaceous aerosols at the top of the atmosphere has warming effects over Asia (+0.21 W m^{-2}), whereas cooling effects occur over South America (−0.47 W m^{-2}) and Africa (−0.12 W m^{-2}) owing to the divergent strengths of black-carbon absorption and organic-carbon scattering.

Plain Language Summary

The tropopause aerosol layer (TAL) defines the accumulation of aerosols in the upper troposphere and lower stratosphere and induces precipitation anomalies, radiation perturbation, and even stratospheric ozone depletion, through which it may contribute to the effects of climate change. Previous studies have shown that the TAL is prevalent over Asia during the summer monsoon period, although it is unclear whether the phenomenon exists in other areas. This study investigated the occurrence of TALs worldwide and found that it is not limited to Asia but is also observed in South America and Africa. The TAL is a result of the combined effects of monsoon dynamics and pollutant emissions, leading to its unique spatial characteristics and radiative effects.

1 Introduction

The tropopause aerosol layer (TAL) defines the accumulation and concentration of aerosols in the upper troposphere and lower stratosphere (Bian et al., 2020; Lau et al., 2018), contrasting with the decreasing concentration of aerosols in the lower troposphere as altitude increases (Liu et al., 2021; Yu et al., 2010). The phenomenon was first discovered over Asia during the boreal summer through satellite retrieval and model simulation and was known as the Asian Tropopause Aerosol Layer (ATAL) (Vernier et al., 2011; Yu et al., 2017). The presence of the ATAL can significantly alter precipitation (Fadnavis et al., 2017), deplete stratospheric ozone (Salawitch and McBride, 2022; Solomon et al., 2022), and inhibit surface warming (Fadnavis et al., 2019), resulting in considerable impacts on the environment, hydrology, and even human life in Asia (Liu et al., 2020; Usha et al., 2022; Yuan et al., 2019b).

The ATAL is formed by the joint effects of monsoon dynamics and surface pollutant emission (Lau et al., 2018; Lelieveld et al., 2018; Yu et al., 2017). Specifically, local emissions and long-range transport by prevailing southwesterly winds lead to high concentrations of surface pollutants over South and East Asia (Neely et al., 2014; Wu et al., 2022b; Zhang et al., 2019). During the Asian Summer Monsoon (ASM) period, deep convection and strong updrafts occur, forcing surface pollutants to penetrate into the stratosphere (Bucci et al., 2020; Lau and Kim, 2022b). ASM anticyclonic circulation in the upper troposphere acts as a trap, causing the pollutants to accumulate over the Tibetan Plateau rather than spreading globally (Vernier et al., 2011; Yuan et al., 2019a). In view of this formation mechanism, the TAL may exist over other areas such as the Australian–Asian, African, and American monsoon regions (Geen et al., 2020). If so, the spatial features of each TAL may be different because each regional monsoon sub-system has unique characteristics of intensity, extent, and prevailing period (Li et al., 2016; Zhisheng et al., 2015). Previous studies have suggested the possible existence of TALs over North America and Africa, but considerable uncertainty remains (Vernier et al., 2015; Yu et al., 2015), so it is necessary to examine the possible existence of TALs worldwide to evaluate their potential atmospheric and climatic effects.

Interactions between aerosols and short-wave radiation significantly impact atmospheric thermodynamic and dynamic states, with notable effects on the radiation budget and climate system (Zhang et al., 2020). In the ATAL, the aerosols have considerable radiative effects, with radiation perturbations of +0.15 W m^{-2} at the top of the atmosphere and −0.72 W m^{-2} at the surface (Geo et al., 2023, JGR), despite their relatively small amounts compared with surface loading. Carbonaceous aerosols (CAs), are prevalent in the ATAL and are particularly important due to their high capacity for solar radiation absorption (Ding et al., 2016; Tao et al., 2020). Radiative forcing (RF) induced by CAs is approximately twice that of mass-equivalent sulfate aerosol (Liu et al., 2022). Atmospheric warming induced by ATAL CAs causes increased precipitation over Asia through strengthening the monsoon Hadley circulation (Fadnavis et al., 2017, ACP). Therefore, it is vital to assess the radiative effects of TAL globally, with a strong focus on CAs because of their widespread distribution in the world, particularly in monsoon regions (Figure S1).

This study aimed to provide a global perspective on the TAL phenomenon by considering its existence in different monsoon regions based on the CAs component. Data from multiple sources including satellite retrievals, re-analysis, and model simulations were used to elucidate processes that influence the formation and evolution of a TAL, particularly the impact of monsoon dynamics and surface pollutants. Our results provide innovative insights into the interactions between aerosols and monsoons, thus contributing to a deeper understanding of these complex phenomena.

2 Data and Methods

2.1 Satellite Retrieval

The Ozone Mapping and Profiler Suite (OMPS) Limb Profiler (LP) aboard the Suomi National Polar-orbiting Partnership satellite was launched in October 2011, aiming to retrieve vertical profiles of ozone, aerosol extinction, and cloud-top height (Chen et al., 2018, 2020). The instrument measures limb-scattering radiance at six wavelengths (510, 600, 675, 745, 869, and 997 nm) in the 0–80 km altitude range. The relatively high vertical and spatial sampling allow detection and tracking of sporadic events when aerosol particles are injected into the tropopause (Wu et al., 2022a). In studying the TAL, this work used the Level-2 swath observation product of the OMPS/LP (Taha et al., 2021).

In addition, aerosol optical depth (AOD) from CALIPSO (Wielicki et al., 2010), land cover and fire monitoring product from the Moderate Resolution Imaging Spectroradiometer (MODIS) instrument (Justice et al., 2002), outgoing longwave radiation (OLR) from US National Oceanic and Atmospheric Administration (NOAA) satellite observations (Gruber and Krueger, 1984), and Global Precipitation Climatology Project (GPCP) combined the satellite retrieval and rain gauge observation (Huffman et al., 1997) were also applied.

2.2 Reanalysis

The Modern Era Retrospective analysis for Research and Applications version 2 (MERRA2) atmospheric reanalysis generated by the US NASA Global Modeling and Assimilation Office provides traditional atmospheric products and chemical compositions for aerosols and greenhouse gases (Buchard et al., 2017; Gelaro et al., 2017). MERRA2 modeling and assimilation have allowed many advances in the understanding of atmospheric chemistry, ozone, and stratosphere processes (Randles et al., 2017). Aerosol and ozone products have proved very helpful in the study of global air pollution, from the troposphere to the stratosphere (Che et al., 2019; Wang et al., 2021), well reproducing the ATAL phenomenon (Lau and Kim, 2022b; Wu et al., 2022b; Yuan et al., 2019a). The aerosol and meteorology-related products were thus used here to explore monsoon influences on the TAL.

The fifth generation European Re-Analysis (ERA5) was developed by the European Centre for Medium-Range Weather Forecasts to model data, physics, and core dynamics to provide a detailed description of the global atmosphere, land surface, and ocean waves (Hersbach et al., 2020). ERA5 meteorological data were also used in this study.

2.3 Model Output

Models of the sixth phase of the Coupled Model Inter-comparison Project (CMIP6) enable long-term simulations and various experiments in reconstructing the historical evolution and future projection of climate change and air pollution (Bauer et al., 2020; Eyring et al., 2016; Zanis et al., 2020). CMPI6 model outputs were used to verify the occurrence of TALs.

2.4 WMMEM and Quantitative Contributions of Factors

Weighted multi-model ensemble means (WMMEMs) were used in model bias correction to reduce errors associated with the inter-model spread of CMIP6 data as follows (Shen et al., 2021):

$$Y(t) = \sum_i W_i X_i \quad (1)$$

where X_i is the output time series of each model, W_i is the weighting of each model error relative to a MERRA2 reference, and $Y(t)$ is the corrected CMIP6 output.

Quantitative contributions of influencing factors were based on the multiple-linear-regression model (Cui et al., 2021; Wu et al., 2021).

2.5 NASA Langley Fu–Liou radiative transfer model

The NASA Langley Fu–Liou radiative transfer model computes broadband solar shortwave and thermal longwave profiles of down-welling and up-welling flux accounting for gas absorption, and absorption and scattering by aerosols and clouds (Balmes et al., 2021; Natarajan et al., 2012). It is a highly modified version of the original model developed by Fu and Liou (Fu et al., 1993). Atmospheric profiles of pressure, temperature, water vapor, and ozone, surface albedo and emission, and aerosol optical depth and vertical profiles were the key input parameters. The Langley Fu–Liou radiative transfer model was adopted for rough evaluation of RF caused by TAL CAs.

3 Results

3.1 TALs Formation in Asia, South America, and Africa

Based on the mechanism of formation of the ATAL, the two primary factors causing the appearance of a TAL are monsoon dynamics and surface pollutants. Monsoon-controlled regions characterized by heavy precipitation are shown in Figure 1a, mainly over the land and ocean in the region 30°N–30°S, with South and East Asia including India and China having the most severe anthropogenic pollution. In contrast, South America, Africa, and Southeast Asia are covered mainly by forest and grassland with pollution arising mainly from natural wildfires (Figure 1c, d). There is relatively little atmospheric pollution over the Caribbean and other ocean areas. The pollution distribution is portrayed well by that of CAs (Figure 1b), which are usually used to identify features of the ATAL (Lau and Kim, 2022a; Yuan et al., 2019a). The presence of tropopause CAs, as indicated by multiple data from OMPS/LP satellite retrieval, MERRA2 reanalysis, and CMIP6 simulation (Figures 2 and S6–S17), indicates the occurrence of TALs over Asia, South America, and Africa. Monsoon dynamics are strong in these areas, and surface pollution levels are high (Figures S2–S5). Caribbean and ocean areas also have strong monsoon dynamics but low surface pollution, so they do not exhibit clear TALs, nor do other monsoon-free but high-surface-pollution areas show evidence of TALs, confirming that monsoon dynamics and surface pollutants are essential for their formation.

The appearance of a TAL has a clear seasonal pattern, as indicated in Figures S6–S17. In Asia, the TAL usually appears during June–September, peaking in July–August, as shown earlier (Yuan et al., 2019a). In South America, the TAL appears during October–December, whereas there are two TAL phenomena in Africa, one in West Africa during February–April, and another in East Africa during February–May. All appearances and intensities of TALs correspond to the evolution of monsoon systems (Figure S5) rather than monthly variations in surface pollution levels (Figures S2–S4). This highlights the dominant role of monsoon dynamics in determining seasonal variations in TALs, as found earlier (Wu et al., 2022b). TAL features in West and East Africa are similar, so only the former region is considered here.

3.2 Divergent Spatial Features of TALs

Spatial distributions and cross-sections of TALs over Asia, South America, and Africa are shown in Figure 2 for July–August, October–December, and February–April, respectively. Here, features of TALs were examined mainly on the basis of MERRA2 and CMIP6 datasets, rather than the OMPS/LP dataset, owing to the low signal/noise ratio caused by cloud cover in the latter. Corresponding CAs AOD is shown in Figure 1e–m, and OLR, OMEGA, and the 200 hPa atmospheric circulation fields are shown in Figure 3, indicating features of deep convention, vertical motion, and anticyclones in the upper troposphere caused by monsoon dynamics.

Among these regions, South America exhibits the most intense surface CAs pollution, and Africa the least. There are two pollution centers in Asia: in India and China. During the prevailing monsoon period, upward vertical motion induced by deep convection carries surface pollutants into the upper troposphere and even the lower stratosphere. The highest TAL CAs intensity was thus observed in South America, while intensities were comparable in Asia and Africa. TAL CAs concentrations in South America were 2–3 times those in Asia and Africa, consistent with patterns of surface pollution. However, TAL altitude was highest in Asia, centered at ~120 hPa, followed by South America (~200 hPa), and Africa (~220 hPa). This is due to the Himalayas and the Tibetan Plateau causing the strongest summer monsoon in South Asia (Boos and Kuang, 2010; Zhang et al., 2012) with the most intensive deep convection and upward vertical motion and upwelling velocities exceeding −0.06 Pa s^{-1} in the core ascent zone. Monsoon dynamics in the other areas are relatively weak, even negligible in Africa relative to Asia. It follows that updrafts account for the suspended height of TALs, and tropopause height alone does not determine the rising altitude of the TAL (Figure 3g–i).

Another interesting distinction between TALs in different areas is their three-dimensional shape. The TAL in Asia has the widest spatial coverage, spanning from the Iranian Plateau to eastern China through an extended upper-tropospheric anticyclonic circulation spanning >60° of longitude. This circulation is strengthened by the heating effect of the Himalayas and the Tibetan Plateau, as documented by Wu et al. (2015). In contrast, anticyclonic circulation over South America and Africa is relatively weak, covering only ~30° of longitude. This acts as a barrier, constraining the TAL to a limited spread, mainly over central South America and West Africa. Of the two TAL centers in Asia, the stronger is over the Tibetan Plateau and the weaker is over southwest China, due to anthropogenic pollution (the primary emission source) being centered over small areas of dense population in India and western China and producing two narrow vertical transport conduits, consistent with Lau et al. (2018). In comparison, surface pollutants in South America and Africa are derived mainly from widespread wildfires across forest and grassland, resulting in one broad vertical transport conduit and a single peak TAL center. Overall, TALs in Asia, South America, and Africa thus exhibit divergent spatial features owing to the combined effects of monsoon dynamics and surface pollutant emissions.

3.3 Divergent Radiative Forcing of TALs

The remarkable features of the TALs result in divergent radiative effects. Based on MERRA2 reanalysis, we evaluated RFs induced by TAL CAs in Asia, South America, and Africa utilizing the Langley Fu–Liou radiative transfer model. TAL CAs over Asia have warming effects on the climate system of +0.21 W m^{-2} at the top of the atmosphere (Figure 4), whereas there are cooling effects of −0.47 and −0.12 W m^{-2} over South America and Africa, respectively. These differences are related to CA composition, which includes black carbon (BC) and organic carbon (OC); the former has a high light-absorption capacity and the latter a predominantly light-scattering capacity. The relative CA contents of BC and OC determine RF magnitude and sign. The amount of BC in TAL over Asia (AOD 0.0026) was higher than that in the South American (AOD 0.0016) and African (AOD 0.0008) TALs. The OC content (AOD 0.0034) over Asia was roughly equivalent to the BC content, but it was much higher over South America (AOD 0.0081) and Africa (AOD 0.0029). Therefore, TAL BC warming effects over South America and Africa were offset by OC cooling effects. In contrast to results at the top of the atmosphere, TAL CAs caused negative RFs at the surface for all three regions owing to absorption and scattering of sunlight by CA leading to less shortwave radiation reaching the surface. Among three regions, the surface RF of TAL CAs was lowest in Africa due to its weaker intensity there. In the atmosphere, Asian TAL CAs had the strongest warming effect because of their higher BC contents. Consistent with the results of Gao et al. (2023), our simulation indicated a positive Asian TAL RF at the top of the atmosphere rather than the negative values reported by Vernier et al. (2015). We found that CA-induced warming effects were stronger than those caused by scattering and absorbing aerosols (+0.15 W m−2; Geo et al., 2023). These results thus reflect the importance of TAL CAs in climate systems relative to other types of aerosol. Moreover, we note that larger amounts of CAs will likely be released to the atmosphere by more frequent and intense wildfires caused by favorable meteorological conditions under global warming (Huang et al., 2023; Pu et al., 2021; Xie et al., 2022; Zheng et al., 2023). More attention should thus be paid to CAs or smoke from wildfires to evaluate their source, transport, radiation, and climate effects.

The intensity of solar shortwave radiation varies with altitude, leading to diverse RFs of equivalent CA concentrations at different altitudes. To better understand this phenomenon and highlight the radiative effects of TAL CAs, we examined equivalent CAs at three altitude levels: upper troposphere (300–100 hPa), middle troposphere (600–400 hPa), and lower troposphere (900–700 hPa). In Asia, the equivalent CA levels changed from warming to cooling effects with decreasing altitude, indicating the relative importance of competitive scattering and absorption of radiation by BC and OC at different altitudes. In South America and Africa, equivalent CAs at different altitudes exhibited consistently negative RFs, but with different intensities. These changes from warming to cooling, and RF intensity, result from competition between BC absorption and OC scattering. However, when only one type of aerosol (BC or OC) is considered, RFs increase with altitude because of the stronger solar shortwave radiation at higher altitudes, thus highlighting the importance of TALs to the climate system.

4 Discussion

This study of the TAL phenomenon in South America and Africa followed the discovery of the ATAL (Vernier et al., 2011) and involved multiple data sources including OMPS/LP satellite retrieval, MERRA2 reanalysis, and CMIP6 simulations. Our findings highlight the critical role of monsoon dynamics and surface pollutant emissions in the formation of TALs, which together cause their divergent spatial features and drive their evolution across these three areas. We emphasize the importance of including natural emissions in future TAL studies owing to the increasing frequency and intensity of wildfires under a global warming scenario (Abram et al., 2021; Huang et al., 2023; You and Xu, 2022). Although our results are robust, the inconsistency in TAL seasonality among the OMPS/LP, MERRA2, and CMIP6 datasets indicates uncertainties due to imperfections in cloud removal in satellite retrieval and limitations in the modeling of stratospheric processes. Therefore, further in-situ observations are required for improvement of understanding of TALs. Overall, this study provides new insights into TALs and should aid further study of interactions between aerosols and monsoons, especially concerning their impact on stratospheric chemistry and climate change (Bian et al., 2020; Salawitch and McBride, 2022; Solomon et al., 2022).

5 Conclusions

This study aimed to investigate the TAL phenomenon by analysis of CAs using multiple data sources including OMPS/LP satellite retrieval, MERRA2 reanalysis, and CMIP6 model outputs. Results indicate that TALs occur not only in Asia, but also in South America and Africa during their monsoon periods. Monsoon dynamics and surface pollutant emissions are the two prime factors involved in TAL formation. The TAL in Asia has the highest altitude and widest spatial coverage due to the effects of strong deep convection, updrafts, and a large anticyclonic system in the upper troposphere, all of which are caused by strong monsoon dynamics. Whereas, TAL intensity was highest in South America due to heavy surface CAs emissions. In Asia, anthropogenic pollution is concentrated over small areas of dense population in India and western China, producing two narrow vertical transport conduits and two TAL centers. In contrast, surface pollutants in South America and Africa are derived mainly from widespread wildfires across forest and grassland, resulting in a broad vertical transport conduit and single TAL peak centers. The divergent features of TALs among the three regions cause distinct RFs. Those at the top of the atmosphere cause warming over Asia (+0.21 W m^{-2}) and cooling over South America (−0.47 W m^{-2}) and Africa (−0.12 W m^{-2}). These opposing RFs result from the different CA compositions of anthropogenic and natural emissions, where the relative amounts of absorbing BC and scattering OC determine the magnitude and sign of the RF. In addition, equivalent CAs at higher altitudes induce larger RFs. These results indicate the important divergent climate effects of TALs over Asia, South America, and Africa.

Open Research

The aerosol extinction ratio from OMPS/LP aboard the S-NPP can be retrieved from https://doi.org/10.5067/CX2B9NW6FI27. The MERRA2 reanalysis is available at the following links: Product inst3_3d_aer_Nv, https://doi.org/10.5067/LTVB4GPCOTK2; instM_3d_asm_Np, https://doi.org/10.5067/2E096JV59PK7; tavgM_2d_aer_Nx, https://doi.org/10.5067/FH9A0MLJPC7N; tavgM_2d_rad_Nx, https://doi.org/10.5067/OU3HJDS973O0. The ERA5 reanalysis is obtained from https://doi.org/10.24381/cds.6860a573. The CMIP6 models' outputs can be found at https://esgf-node.llnl.gov/search/cmip6/. The CALIPSO satellite retrieval (product: LID_L3_Tropospheric_APro_CloudFree-Standard-V4-20) is available at https://opendap.larc.nasa.gov/opendap/CALIPSO/LID_L3_Tropospheric_APro_CloudFree-Standard-V4-20/contents.html. The fire count can be downloaded from the Fire Information for Resource Management System (FIRMS; https://firms.modaps.eosdis.nasa.gov/download/create.php), in which the fire sources from MODIS and VIIRS S-NPP were employed after selecting the file format and submitting the email address. The land cover (product name: MCD12C1, i.e., MODIS/Terra+Aqua Land Cover Type Yearly L3 Global 0.05Deg CMG) from MODIS is available at https://ladsweb.modaps.eosdis.nasa.gov/search/order/1/MCD12C1--6, which can be retrieved from the above link after selecting the product: MCD12C1. The OLR from NOAA and precipitation from GPCP can be obtained from https://psl.noaa.gov/data/gridded/data.olrcdr.interp.html and https://psl.noaa.gov/data/gridded/data.gpcp.html, respectively. The NASA Langley Fu-Liou radiative transfer model can be accessed from https://cloudsgate2.larc.nasa.gov/cgi-bin/fuliou/lflcode/accesslfl.cgi after registration. All data used in this paper are available at the time of submission. Figures in this manuscript were made with python version 3.9 and this software is available from https://www.python.org/.

Acknowledgments

This research was supported by the National Key Research and Development Program of China (2019YFA0606801), the National Science Fund for Distinguished Young Scholars (42025102), the Natural Science Founds of Gansu Province, China (22JR5RA418), and the Fundamental Research Funds for the Central Universities (lzujbky-2022-it05). The calculation was supported by the Supercomputing Center of Lanzhou University.

Conflict of Interest

The authors declare no conflicts of interest relevant to this study.

References

Abram, N. J., Henley, B. J., Sen Gupta, A., Lippmann, T. J., Clarke, H., Dowdy, A. J., et al. (2021). Connections of climate change and variability to large and extreme forest fires in southeast Australia. *Communications Earth & Environment, 2*(1), 8. https://doi.org/10.1038/s43247-020-00065-8

Balmes, K. A., & Fu, Q. (2021). All-sky aerosol direct radiative effects at the ARM SGP site. *Journal of Geophysical Research: Atmospheres, 126*(17), e2021JD034933. https://doi.org/10.1029/2021JD034933

Bauer, S. E., Tsigaridis, K., Faluvegi, G., Kelley, M., Lo, K. K., Miller, R. L., et al. (2020). Historical (1850–2014) aerosol evolution and role on climate forcing using the GISS ModelE2.1 contribution to CMIP6. *Journal of Advances in Modeling Earth Systems, 12*(8), e2019MS001978. https://doi.org/10.1029/2019MS001978

Bian, J., Li, D., Bai, Z., Li, Q., Lyu, D., & Zhou, X. (2020). Transport of Asian surface pollutants to the global stratosphere from the Tibetan Plateau region during the Asian summer monsoon. *National Science Review, 7*(3), 516-533. https://doi.org/10.1093/nsr/nwaa005

Boos, W. R., & Kuang, Z. (2010). Dominant control of the South Asian monsoon by orographic insulation versus plateau heating. *Nature, 463*(7278), 218-222. https://doi.org/10.1038/nature08707

Bucci, S., Legras, B., Sellitto, P., d'Amato, F., Viciani, S., Montori, A., et al. (2020). Deep-convective influence on the upper troposphere–lower stratosphere composition in the Asian monsoon anticyclone region: 2017 StratoClim campaign results. *Atmospheric Chemistry and Physics, 20*(20), 12193-12210. https://doi.org/10.5194/acp-20-12193-2020

Buchard, V., Randles, C. A., Da Silva, A. M., Darmenov, A., Colarco, P. R., Govindaraju, R., et al. (2017). The MERRA-2 aerosol reanalysis, 1980 onward. Part II: Evaluation and case studies. *Journal of Climate, 30*(17), 6851-6872. https://doi.org/10.1175/JCLI-D-16-0613.1

Che, H., Gui, K., Xia, X., Wang, Y., Holben, B. N., Goloub, P., et al. (2019). Large contribution of meteorological factors to inter-decadal changes in regional aerosol optical depth. *Atmospheric Chemistry and Physics, 19*(16), 10497-10523. https://doi.org/10.5194/acp-19-10497-2019

Chen, Z., Bhartia, P. K., Loughman, R., Colarco, P., & DeLand, M. (2018). Improvement of stratospheric aerosol extinction retrieval from OMPS/LP using a new aerosol model. *Atmospheric Measurement Techniques, 11*(12), 6495-6509. https://doi.org/10.5194/amt-11-6495-2018

Chen, Z., Bhartia, P. K., Torres, O., Jaross, G., Loughman, R., DeLand, M., et al. (2020). Evaluation of the OMPS/LP stratospheric aerosol extinction product using SAGE III/ISS observations. *Atmospheric Measurement Techniques, 13*(6), 3471-3485. https://doi.org/10.5194/amt-13-3471-2020

Cui, J., Shi, T., Zhou, Y., Wu, D., Wang, X., & Pu, W. (2021). Satellite-based radiative forcing by light-absorbing particles in snow across the Northern Hemisphere. *Atmospheric Chemistry and Physics, 21*(1), 269-288. https://doi.org/10.5194/acp-21-269-2021

Ding, A. J., Huang, X., Nie, W., Sun, J. N., Kerminen, V. M., Petäjä, T., et al. (2016). Enhanced haze pollution by black carbon in megacities in China. *Geophysical Research Letters, 43*(6), 2873-2879. https://doi.org/10.1002/2016GL067745

Eyring, V., Bony, S., Meehl, G. A., Senior, C. A., Stevens, B., Stouffer, R. J., & Taylor, K. E.

(2016). Overview of the Coupled Model Intercomparison Project Phase 6 (CMIP6) experimental design and organization. *Geoscientific Model Development, 9*(5), 1937-1958. https://doi.org/10.5194/gmd-9-1937-2016

Fadnavis, S., Kalita, G., Kumar, K. R., Gasparini, B., & Li, J. L. F. (2017). Potential impact of carbonaceous aerosol on the upper troposphere and lower stratosphere (UTLS) and precipitation during Asian summer monsoon in a global model simulation. *Atmospheric Chemistry and Physics, 17*(18), 11637-11654. https://doi.org/10.5194/acp-17-11637-2017

Fadnavis, S., Müller, R., Kalita, G., Rowlinson, M., Rap, A., Li, J. L. F., et al. (2019). The impact of recent changes in Asian anthropogenic emissions of SO 2 on sulfate loading in the upper troposphere and lower stratosphere and the associated radiative changes. *Atmospheric Chemistry and Physics, 19*(15), 9989-10008. https://doi.org/10.5194/acp-19-9989-2019

Fu, Q., & Liou, K. N. (1993). Parameterization of the radiative properties of cirrus clouds. *Journal of Atmospheric Sciences, 50*(13), 2008-2025. https://doi.org/10.1175/1520-0469(1993)050<2008:POTRPO>2.0.CO;2

Gao, J., Huang, Y., Peng, Y., & Wright, J. S. (2023). Aerosol Effects on Clear-Sky Shortwave Heating in the Asian Monsoon Tropopause Layer. *Journal of Geophysical Research: Atmospheres, 128*(4), e2022JD036956. https://doi.org/10.1029/2022JD036956

Geen, R., Bordoni, S., Battisti, D. S., & Hui, K. (2020). Monsoons, ITCZs, and the concept of the global monsoon. *Reviews of Geophysics, 58*(4), e2020RG000700. https://doi.org/10.1029/2020RG000700

Gelaro, R., McCarty, W., Suárez, M. J., Todling, R., Molod, A., Takacs, L., et al. (2017). The modern-era retrospective analysis for research and applications, version 2 (MERRA-2). *Journal of Climate, 30*(14), 5419-5454. https://doi.org/10.1175/JCLI-D-16-0758.1

Gruber, A., & Krueger, A. F. (1984). The status of the NOAA outgoing longwave radiation data set. *Bulletin of the American Meteorological Society, 65*(9), 958-962. https://doi.org/10.1175/1520-0477(1984)065<0958:TSOTNO>2.0.CO;2

Hersbach, H., Bell, B., Berrisford, P., Hirahara, S., Horányi, A., Muñoz-Sabater, J., et al. (2020). The ERA5 global reanalysis. *Quarterly Journal of the Royal Meteorological Society, 146*(730), 1999-2049. https://doi.org/10.1002/qj.3803

Huang, X., Ding, K., Liu, J., Wang, Z., Tang, R., Xue, L., et al. (2023). Smoke-weather interaction affects extreme wildfires in diverse coastal regions. *Science, 379*(6631), 457-461. https://doi.org/10.1126/science.add9843

Huffman, G. J., Adler, R. F., Arkin, P., Chang, A., Ferraro, R., Gruber, A., et al. (1997). The global precipitation climatology project (GPCP) combined precipitation dataset. *Bulletin of the American Meteorological Society, 78*(1), 5-20. https://doi.org/10.1175/1520-0477(1997)078<0005:TGPCPG>2.0.CO;2

Justice, C. O., Giglio, L., Korontzi, S., Owens, J., Morisette, J. T., Roy, D., et al. (2002). The MODIS fire products. *Remote sensing of Environment, 83*(1-2), 244-262. https://doi.org/10.1016/S0034-4257(02)00076-7

Lau, W. K., & Kim, K. M. (2022). Recent trends in transport of surface carbonaceous aerosols to the upper-troposphere-lower-stratosphere linked to expansion of the Asian Summer Monsoon Anticyclone. *Journal of Geophysical Research: Atmospheres*, e2022JD036460. https://doi.org/10.1029/2022JD036460

Lau, W. K., Yuan, C., & Li, Z. (2018). Origin, maintenance and variability of the Asian

Tropopause Aerosol Layer (ATAL): the roles of monsoon dynamics. *Scientific Reports, 8*(1), 3960. https://doi.org/10.1038/s41598-018-22267-z

Lelieveld, J., Bourtsoukidis, E., Brühl, C., Fischer, H., Fuchs, H., Harder, H., et al. (2018). The South Asian monsoon—pollution pump and purifier. *Science, 361*(6399), 270-273. https://doi.org/10.1126/science.aar2501

Li, Z., Lau, W. M., Ramanathan, V., Wu, G., Ding, Y., Manoj, M. G., et al. (2016). Aerosol and monsoon climate interactions over Asia. *Reviews of Geophysics, 54*(4), 866-929. https://doi.org/10.1002/2015RG000500

Liu, C. C., Portmann, R. W., Liu, S., Rosenlof, K. H., Peng, Y., & Yu, P. (2022). Significant Effective Radiative Forcing of Stratospheric Wildfire Smoke. *Geophysical Research Letters, 49*(17), e2022GL100175. https://doi.org/10.1029/2022GL100175

Liu, J., Wu, D., Wang, T., Ji, M., & Wang, X. (2021). Interannual variability of dust height and the dynamics of its formation over East Asia. *Science of The Total Environment, 751*, 142288. https://doi.org/10.1016/j.scitotenv.2020.142288

Liu, Y., Li, Y., Huang, J., Zhu, Q., & Wang, S. (2020). Attribution of the Tibetan Plateau to northern drought. *National Science Review, 7*(3), 489-492. https://doi.org/10.1093/nsr/nwz191

Natarajan, M., Pierce, R. B., Schaack, T. K., Lenzen, A. J., Al-Saadi, J. A., Soja, A. J., et al. (2012). Radiative forcing due to enhancements in tropospheric ozone and carbonaceous aerosols caused by Asian fires during spring 2008. *Journal of Geophysical Research: Atmospheres, 117*(D6). https://doi.org/10.1029/2011JD016584

Neely III, R. R., Yu, P., Rosenlof, K. H., Toon, O. B., Daniel, J. S., Solomon, S., & Miller, H. L. (2014). The contribution of anthropogenic SO2 emissions to the Asian tropopause aerosol layer. *Journal of Geophysical Research: Atmospheres, 119*(3), 1571-1579. https://doi.org/10.1002/2013JD020578

Pu, W., Cui, J., Wu, D., Shi, T., Chen, Y., Xing, Y., et al. (2021). Unprecedented snow darkening and melting in New Zealand due to 2019–2020 Australian wildfires. *Fundamental Research, 1*(3), 224-231. https://doi.org/10.1016/j.fmre.2021.04.001

Randles, C. A., Da Silva, A. M., Buchard, V., Colarco, P. R., Darmenov, A., Govindaraju, R., et al. (2017). The MERRA-2 aerosol reanalysis, 1980 onward. Part I: System description and data assimilation evaluation. *Journal of Climate, 30*(17), 6823-6850. https://doi.org/10.1175/JCLI-D-16-0609.1

Salawitch, R. J., & McBride, L. A. (2022). Australian wildfires depleted the ozone layer. *Science, 378*(6622), 829-830. https://doi.org/10.1126/science.add2056

Shen, Z., Duan, A., Li, D., & Li, J. (2021). Assessment and ranking of climate models in Arctic Sea ice cover simulation: From CMIP5 to CMIP6. *Journal of Climate, 34*(9), 3609-3627. https://doi.org/10.1175/JCLI-D-20-0294.1

Solomon, S., Dube, K., Stone, K., Yu, P., Kinnison, D., Toon, O. B., et al. (2022). On the stratospheric chemistry of midlatitude wildfire smoke. *Proceedings of the National Academy of Sciences, 119*(10), e2117325119. https://doi.org/10.1073/pnas.2117325119

Taha, G., Loughman, R., Zhu, T., Thomason, L., Kar, J., Rieger, L., & Bourassa, A. (2021). OMPS LP Version 2.0 multi-wavelength aerosol extinction coefficient retrieval algorithm. *Atmospheric Measurement Techniques, 14*(2), 1015-1036. https://doi.org/10.5194/amt-14-1015-2021

Tao, J., Surapipith, V., Han, Z., Prapamontol, T., Kawichai, S., Zhang, L., et al. (2020). High mass absorption efficiency of carbonaceous aerosols during the biomass burning season in Chiang Mai of northern Thailand. *Atmospheric Environment, 240*, 117821. https://doi.org/10.1016/j.atmosenv.2020.117821

Usha, K. H., Nair, V. S., & Babu, S. S. (2022). Effects of aerosol–induced snow albedo feedback on the seasonal snowmelt over the Himalayan region. *Water Resources Research, 58*(2), e2021WR030140. https://doi.org/10.1029/2021WR030140

Vernier, J. P., Fairlie, T. D., Natarajan, M., Wienhold, F. G., Bian, J., Martinsson, B. G., et al. (2015). Increase in upper tropospheric and lower stratospheric aerosol levels and its potential connection with Asian pollution. *Journal of Geophysical Research: Atmospheres, 120*(4), 1608-1619. https://doi.org/10.1002/2014JD022372

Vernier, J. P., Thomason, L. W., & Kar, J. (2011). CALIPSO detection of an Asian tropopause aerosol layer. *Geophysical Research Letters, 38*(7). https://doi.org/10.1029/2010GL046614

Wang, T., Tang, J., Sun, M., Liu, X., Huang, Y., Huang, J., et al. (2021). Identifying a transport mechanism of dust aerosols over South Asia to the Tibetan Plateau: A case study. *Science of the Total Environment, 758*, 143714. https://doi.org/10.1016/j.scitotenv.2020.143714

Winker, D. M., Pelon, J., Coakley Jr, J. A., Ackerman, S. A., Charlson, R. J., Colarco, P. R., et al. (2010). The CALIPSO mission: A global 3D view of aerosols and clouds. *Bulletin of the American Meteorological Society, 91*(9), 1211-1230. https://doi.org/10.1175/2010BAMS3009.1

Wu, D., Liu, J., Wang, T., Niu, X., Chen, Z., Wang, D., et al. (2021). Applying a dust index over North China and evaluating the contribution of potential factors to its distribution. *Atmospheric Research, 254*, 105515. https://doi.org/10.1016/j.atmosres.2021.105515

Wu, D., Niu, X., Chen, Z., Chen, Y., Xing, Y., Cao, X., et al. (2022). Causes and Effects of the Long-Range Dispersion of Carbonaceous Aerosols From the 2019–2020 Australian Wildfires. *Geophysical Research Letters, 49*(18), e2022GL099840. https://doi.org/10.1029/2022GL099840

Wu, D., Shi, T., Niu, X., Chen, Z., Cui, J., Chen, Y., et al. (2022). Seasonal to sub-seasonal variations of the Asian Tropopause Aerosols Layer affected by the deep convection, surface pollutants and precipitation. *Journal of Environmental Sciences, 114*, 53-65. https://doi.org/10.1016/j.jes.2021.07.022

Wu, G., Duan, A., Liu, Y., Mao, J., Ren, R., Bao, Q., et al. (2015). Tibetan Plateau climate dynamics: recent research progress and outlook. *National Science Review, 2*(1), 100-116. https://doi.org/10.1093/nsr/nwu045

Xie, Y., Lin, M., Decharme, B., Delire, C., Horowitz, L. W., Lawrence, D. M., et al. (2022). Tripling of western US particulate pollution from wildfires in a warming climate. *Proceedings of the National Academy of Sciences, 119*(14), e2111372119. https://doi.org/10.1073/pnas.2111372119

You, C., & Xu, C. (2022). Himalayan glaciers threatened by frequent wildfires. *Nature Geoscience,* 1-2. https://doi.org/10.1038/s41561-022-01076-0

Yu, H., Chin, M., Winker, D. M., Omar, A. H., Liu, Z., Kittaka, C., & Diehl, T. (2010). Global view of aerosol vertical distributions from CALIPSO lidar measurements and GOCART simulations: Regional and seasonal variations. *Journal of Geophysical Research: Atmospheres, 115*(D4). https://doi.org/10.1029/2009JD013364

Yu, P., Rosenlof, K. H., Liu, S., Telg, H., Thornberry, T. D., Rollins, A. W., et al. (2017). Efficient transport of tropospheric aerosol into the stratosphere via the Asian summer monsoon anticyclone. *Proceedings of the National Academy of Sciences, 114*(27), 6972-6977. https://doi.org/10.1073/pnas.1701170114

Yu, P., Toon, O. B., Neely, R. R., Martinsson, B. G., & Brenninkmeijer, C. A. (2015). Composition and physical properties of the Asian tropopause aerosol layer and the North American tropospheric aerosol layer. *Geophysical Research Letters, 42*(7), 2540-2546. https://doi.org/10.1002/2015GL063181

Yuan, C., Lau, W. K., Li, Z., & Cribb, M. (2019). Relationship between Asian monsoon strength and transport of surface aerosols to the Asian Tropopause Aerosol Layer (ATAL): interannual variability and decadal changes. *Atmospheric Chemistry and Physics, 19*(3), 1901-1913. https://doi.org/10.5194/acp-19-1901-2019

Yuan, T., Chen, S., Huang, J., Wu, D., Lu, H., Zhang, G., et al. (2019). Influence of dynamic and thermal forcing on the meridional transport of Taklimakan Desert dust in spring and summer. *Journal of Climate, 32*(3), 749-767. https://doi.org/10.1175/JCLI-D-18-0361.1

Zanis, P., Akritidis, D., Georgoulias, A. K., Allen, R. J., Bauer, S. E., Boucher, O., et al. (2020). Fast responses on pre-industrial climate from present-day aerosols in a CMIP6 multi-model study. *Atmospheric Chemistry and Physics, 20*(14), 8381-8404. https://doi.org/10.5194/acp-20-8381-2020

Zhang, J., Wu, X., Liu, S., Bai, Z., Xia, X., Chen, B., et al. (2019). In situ measurements and backward-trajectory analysis of high-concentration, fine-mode aerosols in the UTLS over the Tibetan Plateau. *Environmental Research Letters, 14*(12), 124068. https://doi.org/10.1088/1748-9326/ab5a9f

Zhang, R., Jiang, D., Liu, X., & Tian, Z. (2012). Modeling the climate effects of different subregional uplifts within the Himalaya-Tibetan Plateau on Asian summer monsoon evolution. *Chinese Science Bulletin, 57*, 4617-4626. https://doi.org/10.1007/s11434-012-5284-y

Zhang, X., Chen, S., Kang, L., Yuan, T., Luo, Y., Alam, K., et al. (2020). Direct radiative forcing induced by light-absorbing aerosols in different climate regions over East Asia. *Journal of Geophysical Research: Atmospheres, 125*(14), e2019JD032228. https://doi.org/10.1029/2019JD032228

Zheng, B., Ciais, P., Chevallier, F., Yang, H., Canadell, J. G., Chen, Y., et al. (2023). Record-high CO2 emissions from boreal fires in 2021. *Science, 379*(6635), 912-917. https://doi.org/10.1126/science.ade0805

Zhisheng, A., Guoxiong, W., Jianping, L., Youbin, S., Yimin, L., Weijian, Z., et al. (2015). Global monsoon dynamics and climate change. *Annual review of earth and planetary sciences, 43*, 29-77. https://doi.org/10.1146/annurev-earth-060313-054623

Figures

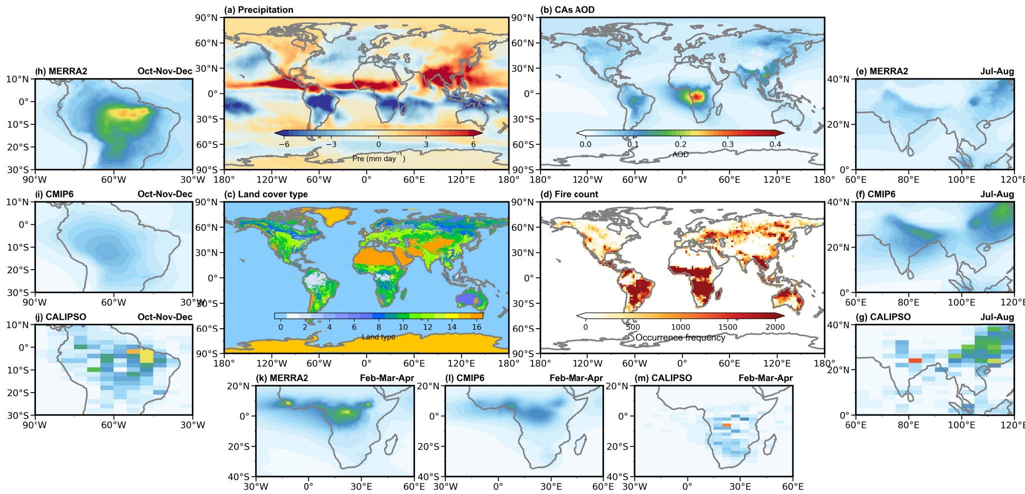

Figure 1. Accumulation regions of carbonaceous aerosols (CAs) and monsoons. **(a)** Spatial distribution of the GPCP precipitation anomaly (mm d^{-1}) between June–September and December–March, 2012–2021. **(b–d)** Spatial distribution of MERRA2 CAs AOD, MODIS land-cover type, and fire frequency, during 2012–2021. **(e–f)** Spatial distribution of CAs AOD over Asia during July–August, 2012–2021 (MERRA2 and CMIP6, respectively). **(g)** Spatial distribution of smoke AOD over Asia, during July–August, 2012–2021 (CALIPSO). **(h–j)** As for (e–g), but for South America during October–December 2012-2021. **(k–m)** As for (e–g), but for Africa during February–April, 2012–2021. In (a) the color bar represents land cover as follows: 0, water; 1, evergreen needle-leaf forest; 2, evergreen broadleaf forest; 3, deciduous needle-leaf forest; 4, deciduous broadleaf forest; 5, mixed forest; 6, closed shrubland; 7, open shrubland; 8, woody savannah; 9, savannah; 10, grassland; 11, permanent wetland; 12, cropland; 13, urban and built-up; 14, cropland/natural vegetation mosaic; 15, snow and ice; and 16, barren or sparsely vegetated. The precipitation anomaly between boreal summer and winter represents the monsoon-prevalent regions. AOD was adopted as a proxy for near-surface CA emission.

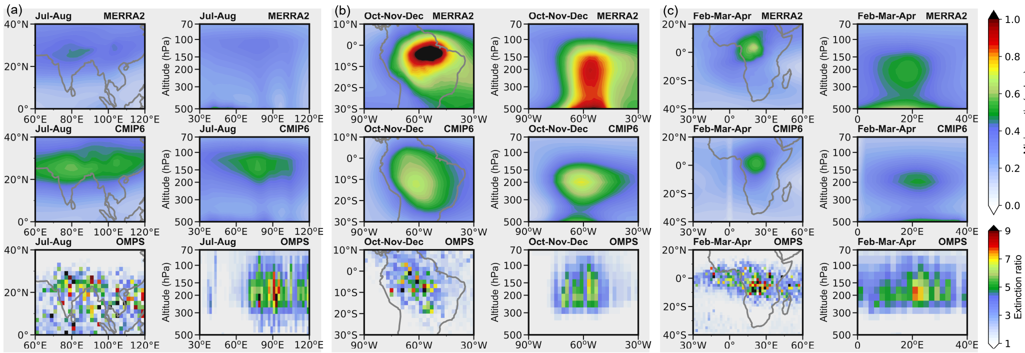

Figure 2. The tropopause aerosols layer (TALs) over Asia, South America, and Africa. (a) Spatial distribution at 80–200 hPa and cross-section over 10°–30°N for the CAs mixing ratio (ppbm; from MERRA2 and CMIP6) and aerosol extinction ratio (OMPS) over Asia, during July–August, 2012–2021. **(b)** Spatial distribution at 150–300 hPa and cross-section over 20°S–0° for the CAs mixing ratio (ppbm; MERRA2 and CMIP6) and aerosol extinction ratio (OMPS) over South America, during October–December, 2012–2021. **(c)** Spatial distribution at 150–250 hPa and cross-section over 10°S–15°N for the CAs mixing ratio (ppbm; MERRA2 and CMIP6) and aerosol extinction ratio (OMPS) over Africa, during February–April, 2012–2021.

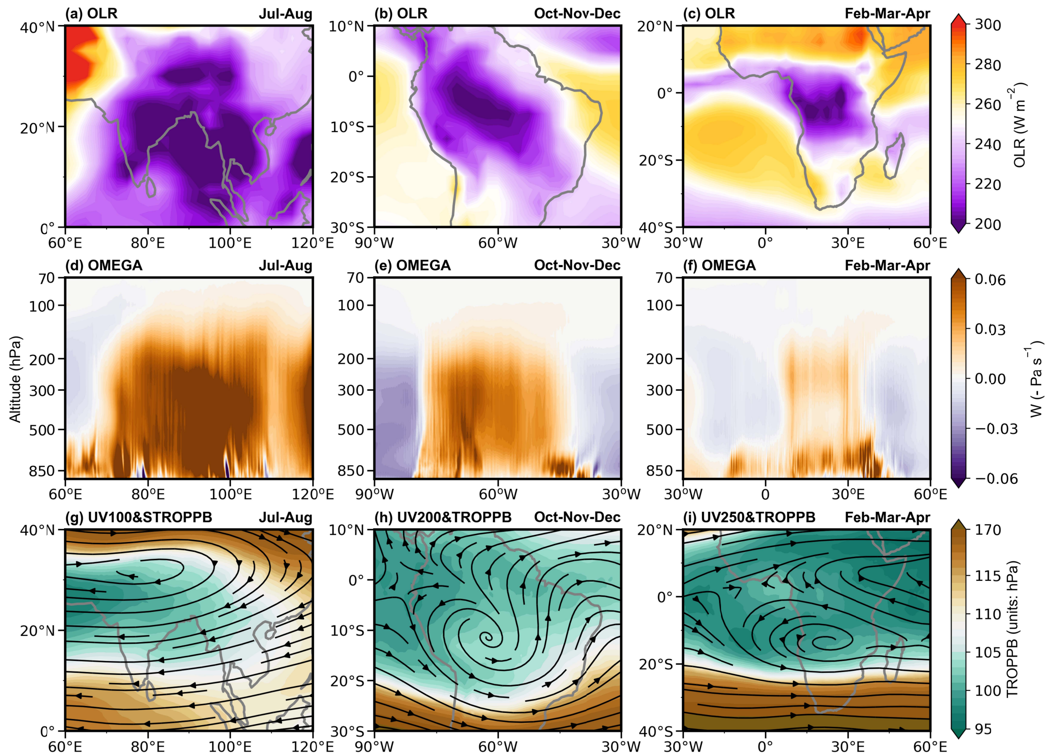

Figure 3. Monsoon dynamic conditions contributing to TALs formation over Asia, South America, and Africa, 2012–2021. (a–c) Spatial distribution of OLR (W m^{-2}; NOAA) during July–August over Asia, October–December over South America, and February–April over Africa. **(d–f)** Cross-section of vertical velocity (−Pa s^{-1}; ERA5) in July–August over 10°–30°N (Asia), October–December over 20°S–0° (South America), and February–April over 10°S–15°N (Africa). **(g–i)** As for (a–c), but for wind field (vectors; ERA5) at 100 hPa (UV100), 250 hPa (UV250), and 200 hPa (UV200), and tropopause pressure based on a blended estimate (TROPPB; hPa, shaded) from MERRA2. OLR was selected as a proxy for deep convection.

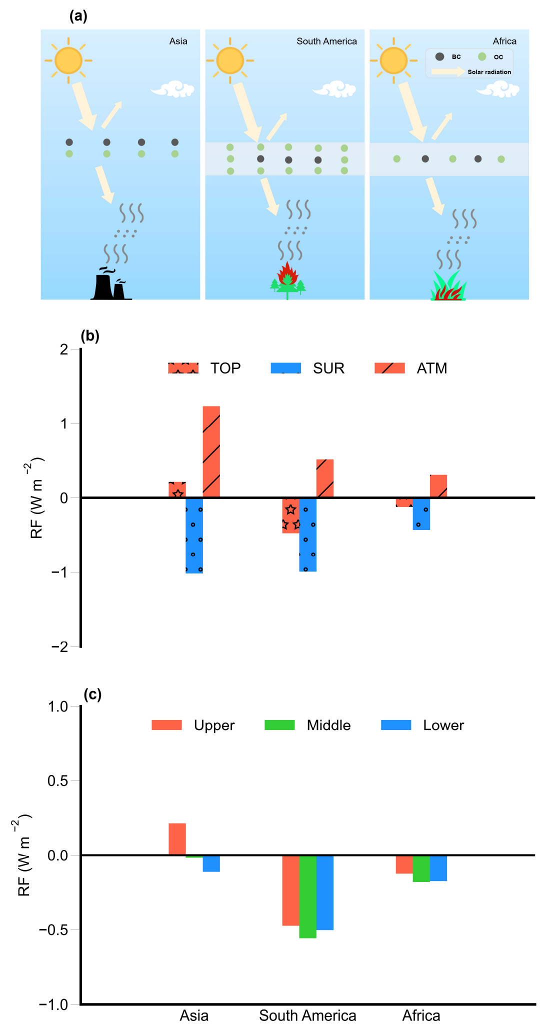

Figure 4. Radiative forcing induced by TALs. (a) The schematic diagram of interactions between solar radiation and CAs (BC and OC) in TALs over Asia, South America, and Africa. **(b)** The radiative forcing (RF, units: W m^{-2}) at the top of the atmosphere (TOP), at the surface (SUR), and in the atmosphere (ATM) induced by TALs over Asia, South America, and Africa. **(c)** The RF at the top of the atmosphere induced by equivalent CAs in the upper troposphere (Upper; red bars), middle troposphere (Middle; green bars), and lower troposphere (Lower; blue bars). TALs CAs mixing ratio (ppbm; CMPI6) over Asia, South America, and Africa were processed for the regions of 15°–0°N and 60°–120°E during July–August over Asia; 20°S–5°N and 70°–35°W during October–December over South America; and 15°S–15°N and 0°–40°E during February–April over Africa.